AAPS PharmSciTech, Vol. 19, No. 6, August 2018 (© 2018)
DOI: 10.1208/s12249-018-1092-2

Research Article

Imidazole-Bearing Polymeric Micelles for Enhanced Cellular Uptake, Rapid Endosomal Escape, and On-demand Cargo Release

Di Lu,[1] Yang An,[1] Simin Feng,[1] Xiaodan Li,[1] Aiping Fan,[1] Zheng Wang,[1,2,3] and Yanjun Zhao[1,3]

Received 4 April 2018; accepted 29 May 2018; published online 18 June 2018

Abstract. The complex design of multifunctional nanomedicine is beneficial to overcome the multiple biological barriers of drug delivery, but it also presents additional hurdles to clinical translation (*e.g.*, scaling-up and quality control). To address this dilemma, we employed a simple imidazole-bearing polymer micelle for enhanced cellular uptake, facilitated endosomal escape, and on-demand release of a model drug, SN-38. The micelles were crosslinked by the reversible imidazole/Zn^{2+} coordination with a drug loading of *ca.* 4% (*w*/*w*) and a diameter less than 200 nm. Under mimicked tumor microenvironment (pH 6.8), the surface charge of micelles reversed from negative to positive, leading to enhanced micelles uptake by model 4T1 cells. Such effect was verified by fluorescent labelling of micelles. Compared to imidazole-free nanocarriers, the charge-reversal micelles delivered significantly more SN-38 to 4T1 cells. Due to the proton sponge effect, imidazole-bearing micelles could rapidly escape from endosomes compared to the control micelles, as evidenced by the kinetic analysis of micelle/endosome co-localization. The coordination crosslinking also enabled the acid-triggered drug release. This work provides a "three birds with one stone" approach to achieve the multifunctionality of nanocarriers without complicated particle design, and opens new avenues of advancing nanomedicine translation *via* simple tailored nanocarriers.

KEY WORDS: micelles; drug delivery; self-assembly; nanocarrier; imidazole.

INTRODUCTION

The employment of nanomedicine and nanotechnology to advance therapeutics delivery has gained intense attention in the past decades, but the clinical translation of nanoformulations is challenging and rare (1–3). Upon dose administration, the nanomedicine must face multiple barriers prior to reaching the target site for the onset of action (4); these include opsonization and clearance of mononuclear phagocyte system, nonspecific distribution, accumulation and penetration in target tissue, cellular uptake, endosomal escape, organelle targeting, drug release, and efflux. Aiming to overcome most of these hurdles, drug delivery nanocarriers are usually featured with a very complex design, termed "multifunctional nanomedicine" (5–7). The integration of imaging and delivery in one nanoplatform (*i.e.*, theranostic nanomedicine) further increased the degree of complexity (8,9). However, the clinical translation of nanomedicine necessitates a simple nanocarrier structure to enable the facile quality control and pilot-scale or large-scale manufacture. This principle is well demonstrated by the success of commercially available nano-products. For example, Doxil® primarily realizes the long circulation of doxorubicin by PEGylation and Abraxane® mainly addresses the poor aqueous solubility of paclitaxel (10,11).

It is appealing to engineer multifunctional nanomedicines with a simple pattern and a high translation potential. Imidazole is a biocompatible small molecule, showing the properties of pH-dependent ionization, reversible coordination with metal ions (*e.g.*, zinc), and reactivity towards free radicals (12–14). It was postulated that nanocarriers with imidazole as one of the building blocks would show improved cellular uptake *via* charge reversal (15), rapid endosomal escape due to proton sponge effect (16,17), and on-demand intracellular drug release as a consequence of reversible ionic crosslinking (18), *i.e.*, an effect of "three birds with one stone" (Scheme 1). Therefore, the aim of this study was to engineer simple imidazole nanocarriers for enhanced drug delivery with high translation potential.

Electronic supplementary material The online version of this article (https://doi.org/10.1208/s12249-018-1092-2) contains supplementary material, which is available to authorized users.

[1] School of Pharmaceutical Science and Technology, Tianjin Key Laboratory for Modern Drug Delivery and High Efficiency, and Collaborative Innovation Center of Chemical Science and Engineering (Tianjin), Tianjin University, 92 Weijin Road, Nankai District, Tianjin, 300072, China.
[2] State Key Laboratory of Medicinal Chemical Biology, Nankai University, Tianjin, 300071, China.
[3] To whom correspondence should be addressed. e-mail: wangzheng2006@tju.edu.cn; zhaoyj@tju.edu.cn)

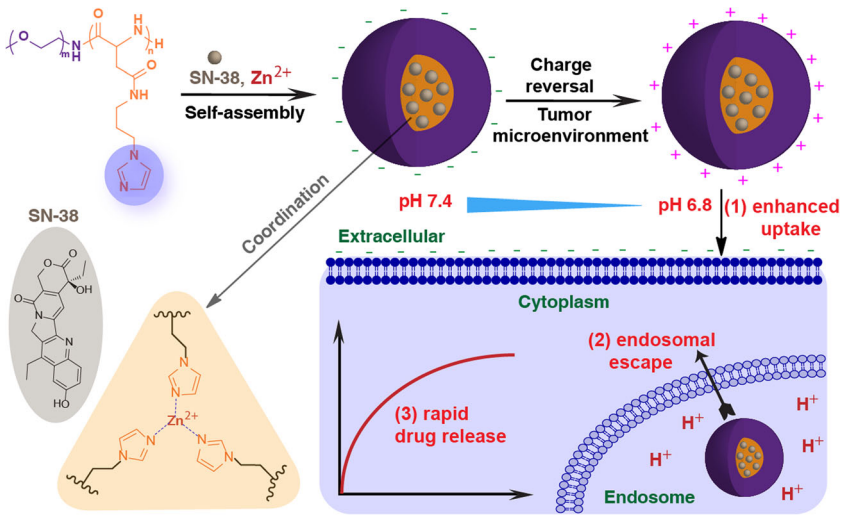

Scheme 1. Illustration of multifunctional imidazole-bearing polymer micelles. In the acidic tumor microenvironment (pH 6.8), the surface charge of micelles was reversed to enhance cellular uptake, followed by rapid endosomal escape through proton sponge effect and on-demand drug release *via* the breaking of imidazole/zinc coordination bonds

Polymeric micelles were selected as the model templates for nanocarrier fabrication by self-assembly in aqueous medium because of the diversity of polymers available and the ease of manipulating nanocarrier properties (*e.g.*, size, shape, and surface chemistry) (7,19).

EXPERIMENTAL

Materials

Disodium hydrogen phosphate, sodium hydroxide (NaOH), citric acid, potassium chloride (KCl), trifluoroacetic acid (TFA), hexane, sodium dodecyl sulfate (SDS), N,N-dimethylformamide (DMF), dichloromethane (DCM), dimethyl sulfoxide (DMSO), tetrahydrofuran (THF), trichloromethane ($CHCl_3$), hydrochloric acid (HCl), and nitrilotriacetic acid (NTA) were purchased from Guangfu Fine Chemical Research Institute (Tianjin, China). Methoxypolyethylene glycol amine (mPEG-NH_2, 5000 Da) was purchased from Beijing JenKem Technology Co., Ltd. (Beijing, China). *L*-Aspartic acid *β*-benzyl ester was obtained from Beijing HWRK Chem Co., Ltd. (Beijing, China). Triphosgene and 1-(3-aminopropyl) imidazole (IM) were acquired from Sigma–Aldrich (Beijing, China). 3-Morpholinopropanesulfonic acid (MOPS) and pyrene were sourced from Jingchun Reagent Co., Ltd. (Shanghai, China). Acetone was purchased from Jiangtian Chemicals (Tianjin, China). Chloroform-d and dimethyl sulfoxide-d_6 (DMSO-d_6) were purchased from Jinouxiang Science and Technology Co., Ltd. (Beijing, China). 7-Ethyl-10-hydroxycamptothecin (SN-38) was obtained from Beijing HVSF United Chemical Materials Co., Ltd. (Beijing, China). Acetonitrile was acquired from Tianjin Concord Technology Co., Ltd. (Tianjin, China). Zinc chloride ($ZnCl_2$) was sourced from Tianjin Yuan Li Chemical Co., Ltd. (Tianjin, China). Murine breast cancer cells (4T1) were obtained from the State Key Laboratory of Medicinal Chemical Biology (Tianjin, China). Roswell Park Memorial Institute (RPMI) 1640, fetal bovine serum (FBS), penicillin-streptomycin (PS), and trypsin-EDTA were purchased from Gibco (Grand Island, USA). Phosphate buffer saline (PBS) and 3-(4,5-dimethyl-2-thiazolyl)-2,5-diphenyl-2-H-tetrazolium bromide (MTT) were purchased from Solarbio Science and Technology Co., Ltd. (Beijing, China). Hoechst 33342 was purchased from Beyotime Institution of Biotechnology (Beijing, China). Chloroquine (CQ) was obtained from Shanghai Macklin Biochemical Co., Ltd. (Shanghai, China). LysoTracker® Red DND-99 was obtained from Yeasen Institution of Biotechnology (Shanghai, China). Bafilomycin A1 (Baf-A1) was purchased from Shanghai Meilune Biotechnology Co., Ltd. (Dalian, China). Cy3 was sourced from Yuanye Bio-Technology Co., Ltd. (Shanghai, China). Paraformaldehyde (4%) was obtained from Solarbio Science and Technology Co., Ltd. (Beijing, China). 4′,6-Diamidino-2-phenylindole (DAPI) was purchased from Beijing Sigma-Aldrich (Beijing, China).

Synthesis of Polymer

Methoxyl poly(ethyl glycol)-poly(*β*-benzyl-*L*-aspartate) (mPEG-PBLA) and methoxyl poly(ethyl glycol)-poly(aspartic acid)-imidazole (mPEG-PAsp-IM) were synthesized according to a recently published method (14). In brief, *L*-aspartic acid *β*-benzyl ester (4 g, 17.92 mmol) and triphosgene (2.64 g, 8.88 mmol) were mixed in 30 mL anhydrous THF under nitrogen protection. The reaction was maintained at 50°C for 3 h. Then, the reaction mixture was evaporated to 8 mL and precipitated by 40 mL precooling hexane. The precipitate was dissolved by anhydrous THF and crystallized by ice-cold hexane. The monomer, benzyl 2-(2,5-dioxooxazolidin-4-yl)acetate (BLA-NCA) was obtained (yield 83%). BLA-NCA (1 g, 4 mmol) and mPEG-NH_2 (0.67 g, 0.13 mmol) were dissolved in 1 mL anhydrous oxygen-free DMF and 10 mL anhydrous $CHCl_3$ under nitrogen protection. The reaction was carried out at 35°C for 24 h, and the mixture was precipitated by 50 mL ice-cold diethyl ether thrice. The sediment was dissolved in DMF and dialyzed against distilled water (molecular weight cutoff/MWCO 3500 Da). Finally, mPEG-PBLA was obtained after

lyophilization (yield 80%). mPEG-PBLA (1 g, 0.1 mmol) and IM (7.16 mL, 60 mmol) were mixed with 10 mL DMSO under nitrogen protection. The mixture was carried out at 40°C for 48 h with constant stirring. Afterwards, the solution was dropped into 30 mL HCl (0.1 M) and dialyzed by HCl (0.01 M) (MWCO 1000 Da). The solution was lyophilized to get final product of mPEG-PAsp-IM (yield 80%) (Scheme S1).

Preparation of Micelles and Drug Encapsulation

7-Ethyl-10-hydroxycamptothecin (SN-38) was chosen as the model drug. The modified thin-film hydration method was used to get the zinc-containing or zinc-free mPEG-PAsp-IM/SN-38 micelles [14]. mPEG-PAsp-IM (200 mg) and SN-38 (20 mg) were dissolved in 30 mL acetonitrile and the solution was evaporated at 50°C to remove the acetonitrile by rotary evaporation. Then, 20 mL MOPS-NaOH buffer solution (pH 7.4, 25 mM) with or without zinc (Zn^{2+}) was used to fully hydrate the film. The solution was collected and further purified by centrifugation, and the supernatant was lyophilized ready for use. The drug loading in mPEG-PBLA employed a similar approach. The SN-38 content in the micelles was determined by dissolving the micelle samples followed by dilution prior to quantification by an Agilent 1200 high-performance liquid chromatography (HPLC) (Agilent Technologies Inc., CA, USA). The elution employed a phenomenex Gemini C18 column (250 mm × 4.6 mm, 5 μm) at 30°C and the mobile phase was the mixture of acetonitrile and water (0.1% TFA) (1:1, *v*/*v*) with a flow rate of 1 mL/min. The injection volume was 20 μL and the ultraviolet detection wavelength was 383 nm. The retention time was 3.89 min. The drug loading was expressed as the mass of SN-38 divided by the mass of micelles ($n = 3$).

Micelle Characterization

The coordination ratio between imidazole and zinc was determined by atomic absorption spectroscopy. mPEG-PAsp-IM-Zn^{2+} micelles (12 mg) were dissolved in 1 mL hydrochloric acid (12 M), and the mixture was stirred at 25°C for 1 h. The zinc concentration was determined by a 180-80 polarized Zeeman atomic absorption spectrophotometer (Hitachi High-Technologies Co. Ltd., Shanghai, China) ($n = 3$). The molar coordination ratio between imidazole and zinc was calculated. The critical micelle concentration (CMC) of mPEG-PBLA and mPEG-PAsp-IM at different pH was determined using pyrene as a fluorescence probe (20,21). In brief, the concentration of micelles in PBS (pH 7.4, 6.8, or 5.5) varied from 0.4 to 400 μg/mL and the concentration of pyrene was fixed at 0.5 μM. The fluorescence spectra were recorded using a FLS980 fluorescence spectrometer (Edinburgh Instruments Ltd., Livingston, UK) with the excitation wavelength of 333 nm and the emission wavelength from 350 to 450 nm. The ratio of sample band intensity at 384 and 373 nm was drawn against the logarithm of the concentration and the flexion point of the curve gave the CMC value. The hydrodynamic diameters and the zeta potential of three types of micelles (mPEG-PBLA, mPEG-PAsp-IM, and mPEG-PAsp-IM/Zn^{2+}) were analyzed in PBS (pH 7.4, 6.8, and 5.5) by a Malvern Zetasizer Nano ZS (Malvern Instrument Ltd., Malvern, UK) at 25°C ($n = 3$). The micelle concentration was fixed at 1 mg/mL. The micelle core size and morphology were determined in PBS at pH 6.8 and 7.4 by JEM-100CX II transmission electron microscope (TEM) (JEOL Ltd., Tokyo, Japan).

In Vitro Drug Release

The *in vitro* SN-38 release experiments from mPEG-PBLA/SN-38, mPEG-PAsp-IM/SN-38, and mPEG-PAsp-IM-Zn^{2+}/SN-38 were studied using static Franz-type diffusion cells at 37°C in PBS (pH 7.4 or 5.5) containing 5% (*w*/*v*) SDS to maintain a sink condition. The experiment duration was 36 h. In brief, 2.3 mg mPEG-PBLA/SN-38, 2.5 mg mPEG-PAsp-IM/SN-38, or 1.7 mg mPEG-PAsp-IM-Zn^{2+}/SN-38 in 2 mL PBS (pH 7.4 or 5.5) was transferred to the donor compartment. The receiver fluid was the same buffer system (pH 7.4 or 5.5) with 5% (*w*/*v*) SDS. The donor and receiver compartment were separated by a regenerated cellulose membrane (MWCO 1000 Da). The release medium was agitated at a speed of 250 rpm at 37°C. At desired time intervals, 0.5 mL of release media was withdrawn for drug quantification by HPLC and an equal volume of fresh medium was supplemented instantly. The release experiments were conducted in triplicate and the results were presented as the cumulative drug release against time.

Cytotoxicity Study

Murine breast cancer cells (4T1) were cultured in RPMI 1640 medium containing 10% (*v*/*v*) fetal bovine serum and 1% (*v*/*v*) penicillin-streptomycin under 37°C and 5% CO_2 condition. 4T1 cells were seeded on 96-well plates at 5×10^3 cells per well and cultured for 24 h. Free SN-38, mPEG-PBLA/SN-38, mPEG-PAsp-IM/SN-38, and mPEG-PAsp-IM-Zn^{2+}/SN-38 were added at pH 7.4 or 6.8 with equivalent SN-38 concentrations ranging from 1 to 20 μM. After 6 h's incubation, the medium was replaced with fresh medium at pH 7.4 and incubated for another 24 h. The cell viability was analyzed using the standard MTT assay (22) and the mean half maximal inhibitory concentration (IC_{50}) value ± standard deviation was determined ($n = 4$). The cytotoxicity of placebo micelles (mPEG-PBLA, mPEG-PAsp-IM, and mPEG-PAsp-IM-Zn^{2+}) was also investigated at pH 7.4 and 6.8 using the same MTT approach.

Cellular Uptake of Fluorescent Micelles

To track the intracellular location of micelles, the polymers were labeled with a model fluorescence probe, fluorescein isothiocyanate (FITC), at the polymer backbone terminal position, *i.e.*, mPEG-PBLA-FITC and mPEG-PAsp-IM-FITC. 4T1 cells were seeded on 20-mm plates at 8×10^4 cells/well and cultured for 24 h. The medium was removed, followed by the addition of fresh medium (pH 7.4 or 6.8) containing mPEG-PBLA-FITC (20 μM) and mPEG-PAsp-IM-FITC/Zn^{2+} (20 μM). After 6 h's incubation, the cells were washed by PBS three times, and then the nuclei were stained with Hoechst 33342. After 10 min, the unbound dyes were removed followed by fresh medium supplementation. The intracellular location of micelles was

observed by a LSM710 confocal laser scanning microscope (CLSM) (Carl Zeiss Meditec. Inc., Germany) with the excitation wavelength at 488 nm.

Intracellular Delivery of SN-38

4T1 cells were seeded on 20-mm plates at a density of 8×10^4 cells per well and incubated for 24 h. The original medium was replaced by fresh serum-free medium at pH 7.4 or 6.8. The test samples included mPEG-PBLA/SN-38, mPEG-PAsp-IM/SN-38, mPEG-PAsp-IM-Zn^{2+}/SN-38, and free SN-38; SN-38 dose was fixed at 10 μg/mL for all samples. The cells were incubated for 6 h, and then washed with PBS three times, followed by the addition of fresh medium. The intracellular distribution of SN-38 was observed by CLSM with the excitation wavelength at 405 nm. In addition, the quantitative uptake of SN-38 from different formulations by 4T1 cells was also investigated by HPLC. In brief, the sample-treated cells were digested by trypsin prior to sonication treatment and centrifugation ($8000 \times g$). The supernatant was treated with dichloromethane and centrifuged ($8000 \times g$) before SN-38 quantification by HPLC. The mass ratio of delivered SN-38 with reference to supplemented dose was calculated to assess the degree of SN-38 uptake by cells ($n = 3$).

Endosomal Escape Assessment

4T1 cells were seeded on 20-mm plates at a density of 8×10^4 cells per well for 24 h, and then incubated with either mPEG-PBLA-FITC (20 μM) or mPEG-PAsp-IM-FITC/Zn^{2+} (20 μM) for pre-determined time (2, 4, 6, and 8 h). In addition, the cells were incubated with mPEG-PBLA-FITC (20 μM) or mPEG-PAsp-IM-FITC/Zn^{2+} (20 μM) in the presence of chloroquine (1 μM) for 6 h. LysoTracker® Red DND-99 (50 nM) in FBS-free medium was added to stain lysosomes. After 30 min, the unbound dyes were removed and fresh medium was added. The co-localization of micelles and lysosomes was assessed by CLSM. Green FITC was excited at 488 nm and red LysoTracker was observed using a 561-nm excitation wavelength.

To further prove the endosomal escape ability of imidazole-bearing micelles, the 4T1 cells were treated with micelles as well as bafilomycin-A1 (Baf-A1) to block the development of endosomes to lysosomes (23). In brief, 4T1 cells were seeded on 20-mm plates at a density of 8×10^4 cells per well. After 24 h, the cells were co-incubated with mPEG-PAsp-IM-FITC/Zn^{2+} (20 μM) and Baf-A1 (200 nM) together for 6 or 8 h. Then, the LysoTracker® Red DND-99 (50 nM) in FBS-free medium was added to stain lysosomes for 30 min. The co-localization analysis between micelles and lysosomes was carried out by CLSM. Green FITC was excited at 488 nm and red LysoTracker was observed using a 561-nm excitation wavelength. The presence of Baf-A1 (200 nM) on micelle (mPEG-PAsp-IM-Zn^{2+}/SN-38) cytotoxicity was also investigated using the same MTT approach.

The fluorescence resonance energy transfer (FRET) technique was used to monitor the intracellular integrity of FITC-labeled micelles with FITC and Cy3 as the FRET donor and acceptor, respectively. The Cy3 probe was physically encapsulated in mPEG-PBLA-FITC or mPEG-PAsp-IM-FITC/Zn^{2+} micelles by a typical thin-film hydration method. The probe loading was quantified through fluorescent method (Ex = 545 nm; Em = 565 nm). 4T1 cells at a density of 8×10^4 cells per well were incubated with the micelles at fixed Cy3 dose of 10 μg/mL for 4 h. Then, the excess micelles were removed and rinsed by PBS in triplicate. The cells were fixed using 1 mL paraformaldehyde (4%) for 20 min and stained by DAPI for 10 min. The FRET images were collected by UltraView Vox CLSM (PerkingElmer, USA). The excitation/emission wavelength was 405 nm/415–475 nm (DAPI), 488 nm/580–650 nm (FITC), and 561 nm/580–650 nm (Cy3), respectively.

Buffering Capacity of Imidazole-Bearing Micelles

The buffering capacity of the imidazole-bearing micelles (mPEG-PAsp-IM-Zn^{2+}) and control micelles (mPEG-PBLA) was investigated using a previously published method (24). Both types of micelle aqueous solutions (0.5 mg/mL) were prepared and the pH was adjusted to 10 using NaOH (1 M). The micellar solution was titrated with 0.1 M HCl and the pH of the obtained mixture was recorded continuously. The titration curve was obtained *via* plotting the system pH against the volume of HCl.

Statistical Analysis

All data were presented as mean ± standard deviation (SD). A statistically significant difference was determined at a minimal level of significance of 0.05. Student's *t* test was used for the analysis.

RESULTS AND DISCUSSION

In the current work, the biocompatible methoxy poly(ethylene glycol)-*co*-poly(aspartic acid) was selected as the backbone and imidazole was covalently linked to the side chain *via* aminolysis based on our recently published work (Scheme S1) (14). The generated polymeric conjugate, *i.e.*, methoxyl poly(ethyl glycol)-poly(aspartic acid)-imidazole (mPEG-PAsp-IM) had a molecular weight (MW) of 9400 Da and the corresponding control polymer, methoxyl poly(ethyl glycol)-poly(*β*-benzyl-*L*-aspartate) (mPEG-PBLA) displays a MW of 9100 Da (14). The MW of mPEG was 5000 Da for both polymers. A hydrophobic anticancer agent, SN-38 was chosen as the model drug and zinc (Zn^{2+}) was used as the biocompatible coordination linker (25). Zn^{2+} was employed to produce the imidazole-metal coordination bond and thus to stabilize the mPEG-PAsp-IM micelles *via* ionic crosslinking (26). The IM/Zn^{2+} coordination ratio was determined at 3.0 ± 0.2. The SN-38 loading in micelles was 3.8 ± 0.2% (*w*/*w*) (mPEG-PAsp-IM-Zn^{2+}), 2.7 ± 0.3% (*w*/*w*) (mPEG-PAsp-IM), and 1.5 ± 0.1% (*w*/*w*) (mPEG-PBLA), respectively. The relatively higher drug loading in imidazole-bearing micelles was presumed due to the polymer-drug hydrophobic interaction as well as the potential hydrogen bonding between imidazole (H acceptor) and SN-38 (H donor) (27). Imidazole-zinc coordination further increased drug loading to *ca.* 4.0% (*w*/*w*) due to the presence of crosslinking network, maintenance of micelle stability, and hence avoidance of cargo leakage. A similar effect was

observed in other types of coordination-bonded micelles (18). Micelles undergo a dynamic equilibrium between unimer and assembly state, which to a certain extent influences the loading capability. The coordination crosslinking circumvents this equilibrium, resulting a relatively higher SN-38 loading.

As an indicator of micelle stability, the CMC of the zinc-free micelles mPEG-PAsp-IM was 11.4 ± 0.6 μg/mL (pH 7.4), 23.7 ± 1.2 μg/mL (pH 6.8), and 44.9 ± 0.9 μg/mL (pH 5.5), and the CMC of the control micelles mPEG-PBLA was 10.6 ± 0.3 μg/mL (pH 7.4), 11.1 ± 0.6 μg/mL (pH 6.8), and 11.5 ± 0.7 μg/mL (pH 5.5), respectively, with the help of fluorescence probe (Fig. I). With the pH decreasing, the CMC of mPEG-PAsp-IM showed a slight increase while that of the control did not. In general, the higher the CMC value, the lower the micelle stability (21). The compromised micelle stability with increasing medium acidity was due to the enhanced ionization of imidazole (pKa = 6.9) at the lower pH conditions. Hence, the hydrophobicity of PAsp-IM segment was the lowest at pH 5.5. Since the driving force of micelle formation is the hydrophobic interaction (28), the decrease of PAsp-IM hydrophobicity results in a less stable micelle at lower pH. The hydrodynamic size of both imidazole-bearing types of micelles increased with decreasing pH from 7.4 to 5.5 (Fig. II) (Table S1). Both the CMC reduction and particle size increase at acidic conditions were a consequence of the decline of the driving force of micelle self-assembly, *i.e.*, the diminishment of hydrophobic interactions. Without the PAsp-IM segment, the hydrodynamic size of the control micelles (mPEG-PBLA) mainly kept unchanged (Fig. II) (Table S1). In terms of TEM images, mPEG-PAsp-IM formed spherical micellar nanocarrier irrespective of zinc crosslinking at both pH 6.8 and pH 7.4 (Fig. II). The presence of IM/Zn^{2+} coordination generated a more compact micellar core in contrast to that of zinc-free micelles. The differences between the control micelles and the imidazole-bearing micelles in particle size at different pH also arose from the unique pKa of imidazole, which concurred well with the stability data. The zeta potential of the control micelles mPEG-PBLA was not influenced by the lower pH environment (Fig. III) (Table S1). The surface charge of both crosslinked and non-crosslinked micelles reversed from negative (pH 7.4) to positive (pH 5.5) as a result of imidazole ionization variation (Fig. III) (Table S1), which agreed with the previous report of poly(histidine)-based nanocarriers (15). Since the tumor is

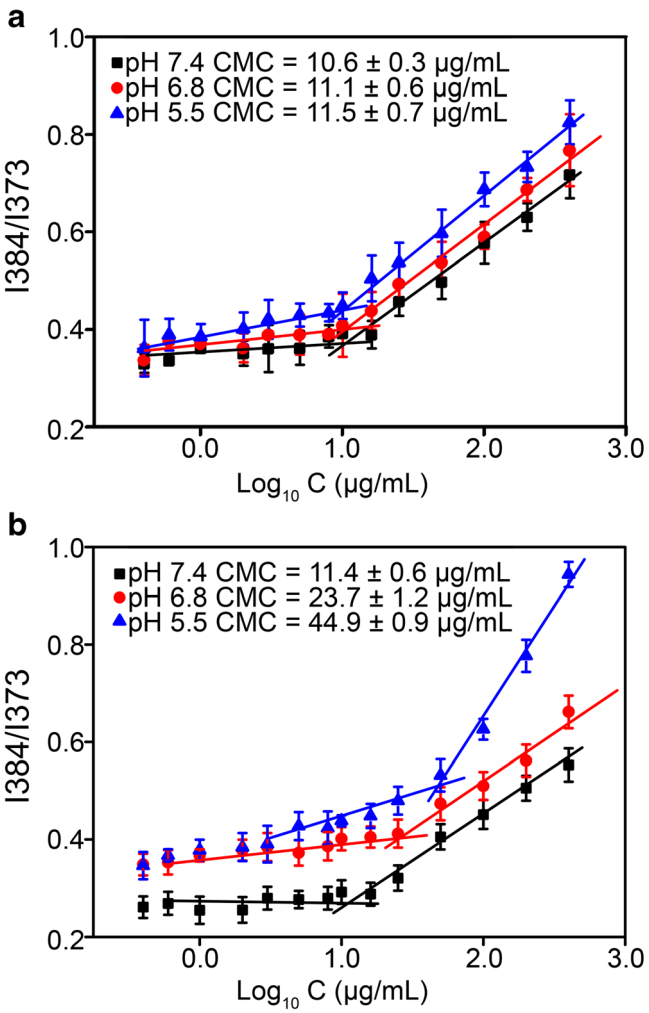

Fig. I. Critical micelle concentration (CMC) of mPEG-PBLA micelles (**a**) and mPEG-PAsp-IM micelles (**b**) at pH 7.4, 6.8, and 5.5

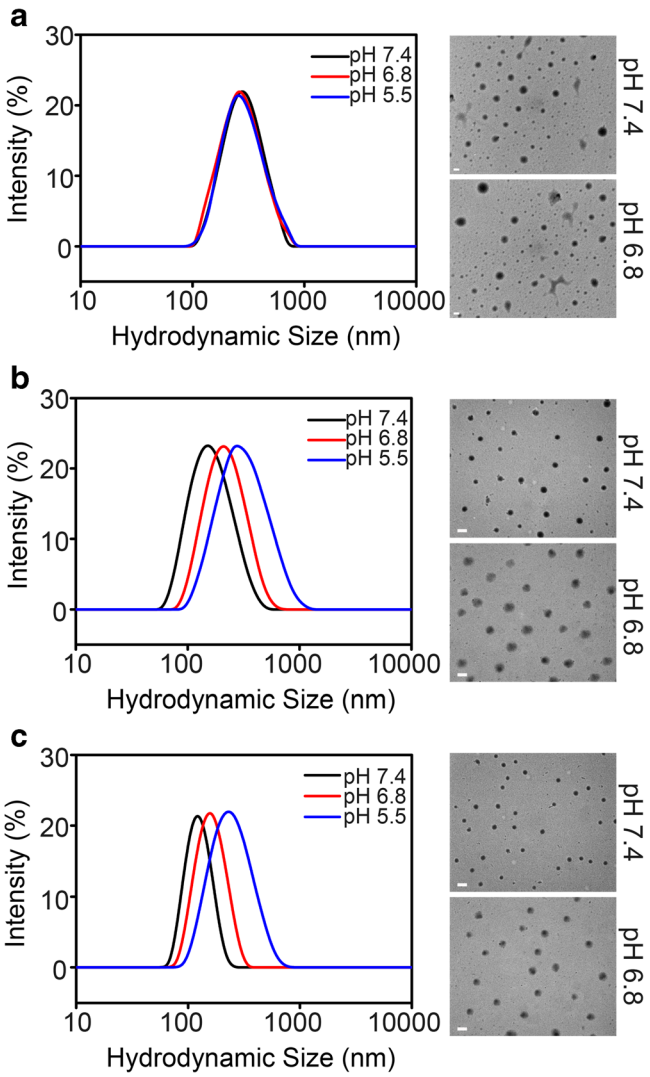

Fig. II. Hydrodynamic sizes and TEM images of mPEG-PBLA micelles (**a**) and mPEG-PAsp-IM micelles without (**b**) and with Zn^{2+} crosslinking (**c**). Scale bar: 200 nm

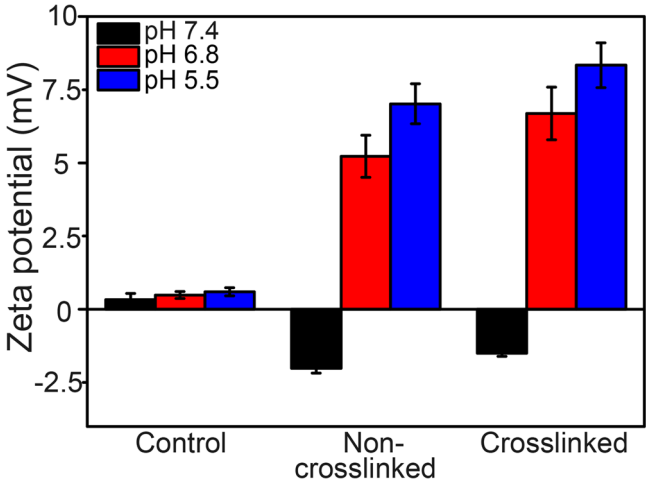

Fig. III. Zeta potential of the control micelles mPEG-PBLA, non-crosslinked mPEG-PAsp-IM micelles, and Zn^{2+} crosslinked mPEG-PAsp-IM micelles at pH 7.4, 6.8, and 5.5 ($n = 3$)

characterized with an acidic microenvironment with pH of *ca.* 6.8, such property would enhance the micelle internalization by cells due to the electrostatic interaction between cationic nanocarrier and negatively charged cell membrane (29,30).

The *in vitro* drug release was carried out under a sink condition *via* the supplementation of 5% (*w*/*v*) sodium dodecyl sulfonate (SDS) to increase the aqueous solubility of SN-38. At neutral pH 7.4, the rate and extent of drug release from crosslinked mPEG-PAsp-IM micelles were lower compared to those from the corresponding non-crosslinked micelles (Fig. IV). Such trend was also consistent at a lower pH at 5.5. This phenomenon was anticipated that the coordination crosslinking well maintained the micelle integrity so that slowed down SN-38 release. From pH 7.4 to pH 5.5, the release rate from control micelles was not statistically different, while there was a dramatic difference between the release curves for both imidazole-bearing samples. The more rapid drug liberation from nanocarriers was a consequence of partial breaking down of coordination bonding at acidic conditions, which caused the collapse of micelles. Such feature is beneficial to minimize premature drug release during systemic circulation and achieve fast dose liberation in the acidic endosome/lysosome to enable rapid onset of drug action inside cells.

In vitro cytotoxicity study of SN-38 in different formulations at different pH was analyzed by MTT assay on 4T1 cells (Fig. V). Free SN-38 exhibited the same cytotoxicity in 4T1 cells regardless of the pH of culture medium (pH 7.4 *vs* pH 6.8). Similarly, the half maximal inhibitory concentration (IC_{50}) of mPEG-PBLA micelles was also not dependent on pH. On the contrast, the pH indeed made a difference to the cytotoxicity of uncrosslinked mPEG-PAsp-IM micelles with a lower IC_{50} at pH 6.8 compared to that at pH 7.4 ($p < 0.05$). The same trend was observed for the Zn^{2+}-crosslinked mPEG-PAsp-IM micelles. This could be explained that the positively charged imidazole-bearing micelles at pH 6.8 were more readily internalized by cells than the micelles at pH 7.4. Hence, an improved cytotoxicity against 4T1 cells was observed, which concurred well the previous investigations (22). As a control, the placebo mPEG-PBLA micelles are not cytotoxic at pH 7.4; the placebo imidazole-bearing micelles

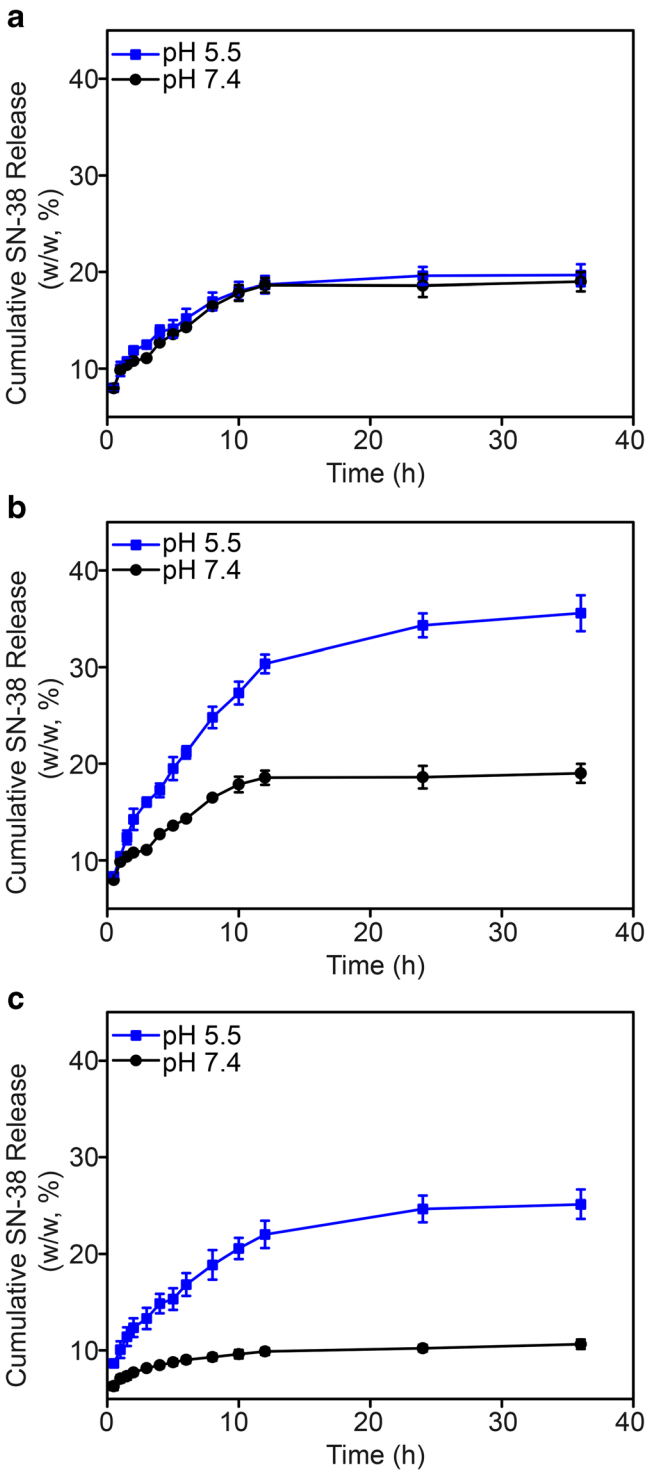

Fig. IV. Cumulative SN-38 release from **a** mPEG-PBLA/SN-38 control micelles, **b** mPEG-PAsp-IM/SN-38 non-crosslinked micelles, and **c** mPEG-PAsp-IM-Zn^{2+}/SN-38 crosslinked micelles at pH 7.4 and 5.5

with or without zinc (*i.e.*, mPEG-PAsp-IM and mPEG-PAsp-IM/Zn^{2+}) did not show cytotoxicity at both pH 7.4 and 6.8 (Figure S1). This might be due to the relatively low ionization degree of polymer at pH 6.8.

To investigate the influence of imidazole on the cellular uptake of micelles, both mPEG-PAsp-IM and mPEG-PBLA

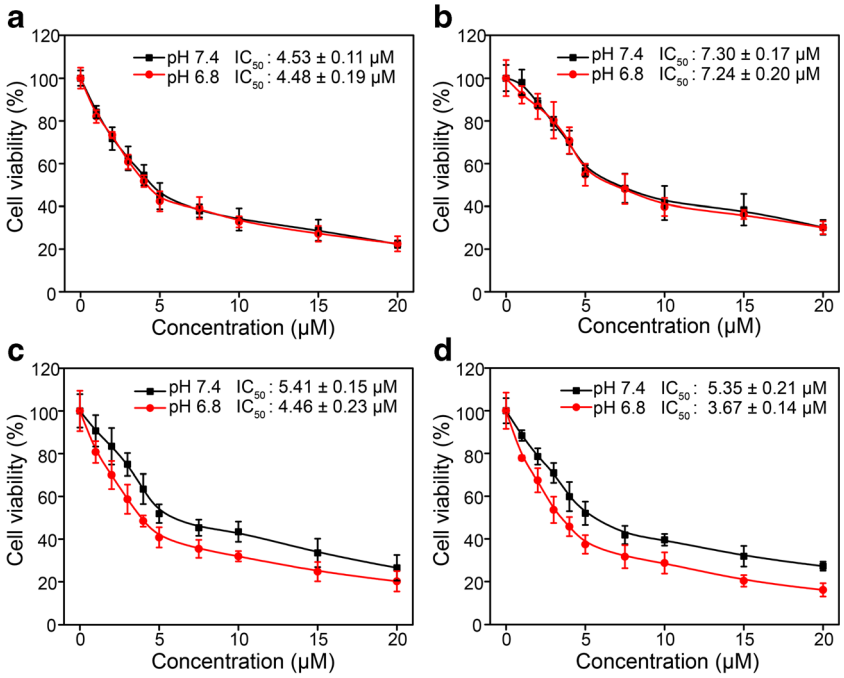

Fig. V. Cytotoxicity of SN-38 in different formulations at pH 7.4 and 6.8 against 4T1 cells: **a** Free SN-38; **b** mPEG-PBLA/SN-38; **c** mPEG-PAsp-IM/SN-38; and **d** mPEG-PAsp-IM-Zn^{2+}/SN-38

was chemically labeled with a fluorescent probe (FITC) at the terminal site, *i.e.*, mPEG-PAap-IM-FITC and mPEG-PBLA-FITC (Figure S2) (31). As FITC was chemically linked to the polymer, the green fluorescence indicated the location of micellar nanocarriers. The fluorescence intensity of mPEG-PAap-IM-FITC/Zn^{2+} micelles was much stronger when the medium pH was maintained at 6.8, compared to that at the neutral culturing conditions (pH 7.4) ($p < 0.05$) (Fig. VI). In contrast, this phenomenon was not evident for the control mPEG-PBLA-FITC micelles ($p > 0.05$). It was believed that the charge-reversal effect of imidazole-bearing nanocarrier induced the electrostatic interaction with negatively charged cell membrane and hence resulted in an enhanced cellular internalization in acidic tumor microenvironment (pH = 6.8). The charge reversal has been a robust approach to enhance the uptake of different types of nanocarriers in a variety of cells (22,32,33). Likewise, non-crosslinked and crosslinked mPEG-PAap-IM micelles both could transport more SN-38 into 4T1 cells at slightly acidic culturing conditions (pH 6.8) compared to that at neutral medium *via* the charge-reversal mechanism (Fig. VII). On the contrary, mPEG-PBLA micelles did not show such ability because of no electrostatic interaction between particles and cell membrane. These data concurred well with the cytotoxicity results (Fig. V).

To assess the endosomal escape behavior of imidazole-bearing micelles, mPEG-PAap-IM-FITC/Zn^{2+} and mPEG-PBLA-FITC nanocarriers were incubated with 4T1 cells for different durations. At pre-determined time points (2, 4, 6, and 8 h), co-localization analysis was performed to examine the degree to micelles and lysosomes overlap (Fig. VIII) (34).

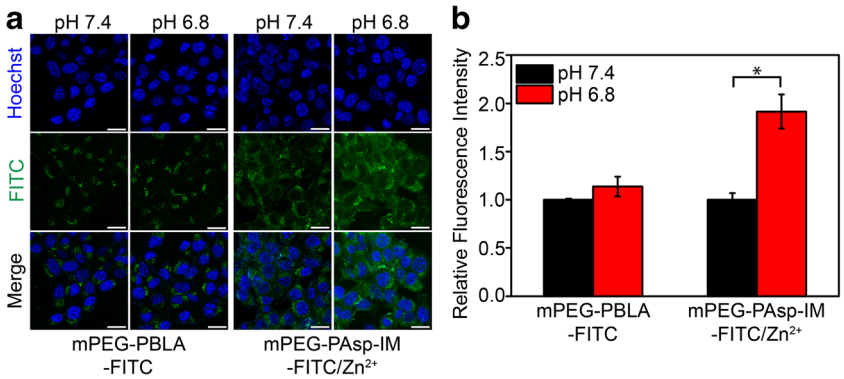

Fig. VI. **a** Confocal laser scanning microscope images of 4T1 cells treated by mPEG-PBLA-FITC and mPEG-PAsp-IM-FITC/Zn^{2+} micelles (both at 20 μM) at pH 7.4 and 6.8, respectively. Nucleus was stained by Hoechst. Scale bar: 20 μm. **b** Semi-quantitative presentation of green fluorescence intensity extracted from confocal images ($n = 3$). *$p < 0.05$

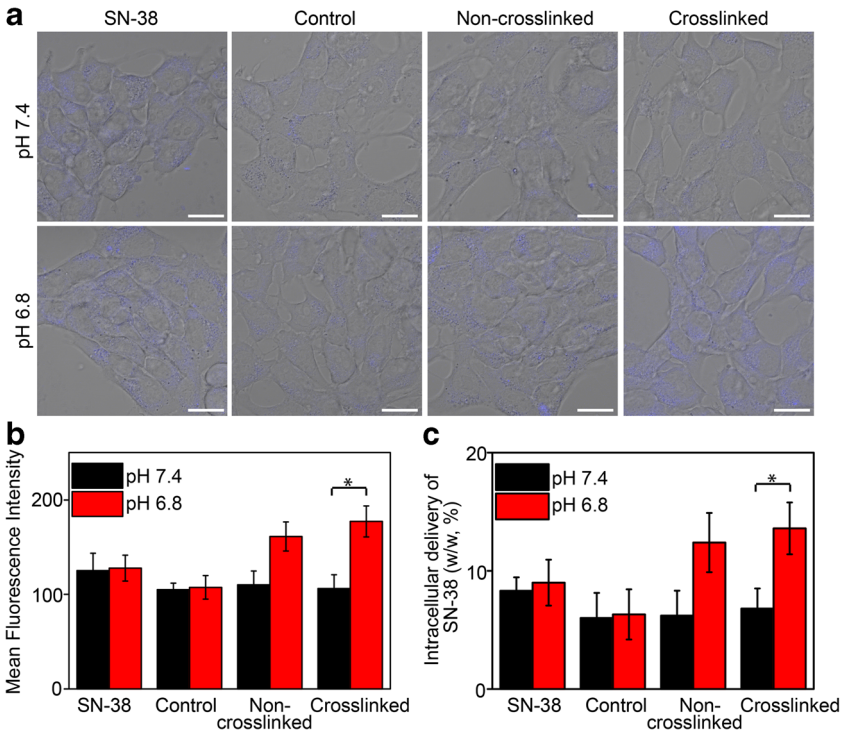

Fig. VII. **a** Uptake of SN-38 (10 μg/mL) of four formulations in 4T1 cells at different pH conditions: free SN-38, the control micelles mPEG-PBLA/SN-38, non-crosslinked micelles mPEG-PAsp-IM/SN-38, and crosslinked micelles mPEG-PAsp-IM-Zn^{2+}/SN-38. SN-38 was excited at 405 nm (blue). Scale bar: 20 μm. **b** Semi-quantitative presentation of SN-38 fluorescence intensity extracted from confocal images ($n = 3$). **c** The mass ratio of delivered SN-38 (10 μg/mL) of four formulations in 4T1 cells at different pH conditions by HPLC analysis ($n = 3$). *$p < 0.05$

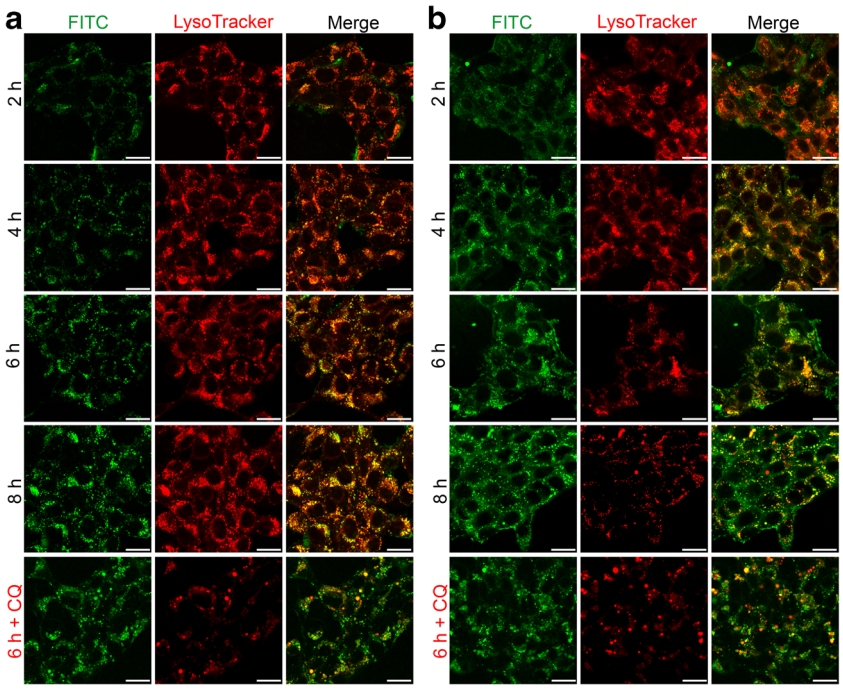

Fig. VIII. The intracellular uptake and kinetic distribution of mPEG-PBLA-FITC micelles (**a**) and mPEG-PAsp-IM-FITC/Zn^{2+} micelles (**b**) in 4T1 cells by CLSM (micelle dose 20 μM) at 2, 4, 6, 8 h and in the presence of chloroquine. The green and red fluorescence represents micelles and lysosomes, correspondingly. Scale bar: 20 μm

The green fluorescence indicated the location of micellar nanocarriers, which was demonstrated by the FRET analysis (Fig. S3). The red fluorescence from commercial probe (LysoTracker® Red DND-99) denoted the site of lysosomes. As a result of micelle and lysosome co-localization, the overlay of green and red color produced yellow color. Regarding mPEG-PBLA-FITC micelles, the extent of co-localization remained high during the time course of experiment (*i.e.*, 8 h), which indicated a low degree of endosomal escape. Nevertheless, for mPEG-PAsp-IM-FITC/Zn^{2+} micelles, the intensity of yellow color reached peak at 4 h, followed by continued drop from 6 to 8 h. This is a typical signal of facilitated endosomal escape. Chloroquine is an endosomolytic agent (35). With the help of chloroquine, co-localization of the control micelles decreased at 6 h and that of the imidazole-bearing micelles was also lower than before. Such trend was semi-quantitatively assessed by Pearson's correlation coefficient (r) (Fig. S4) (36). The value of r ranges from -1 to $+1$; $+1$ indicates a positive linear correlation and -1 signifies a negative linear correlation. The r value of control micelles experienced a steady increase from 2 h to 8 h, implying poor release of nanocarriers from endosomes. In contrast, the r value of imidazole-bearing micelles was the highest at 4 h and then started to drop, demonstrating efficient nanocarrier escape from endosomal organelle. The ability of imidazole to enable endosomal escape was thought as a consequence of a "proton sponge effect" (17,31). Briefly, the ionization of functional moiety (*e.g.*, imidazole) within the acidic endosomes brought large amount of counter ion (*e.g.*, Cl^{-1}) and water, which gradually built up internal pressure within endosomes. Eventually, endosomes were ruptured upon reaching a threshold pressure. Therefore, the number of lysosomes dramatically reduced upon the treatment of imidazole-bearing micelles, which was evidenced by the decrease of red fluorescence from 4 h to 8 h (Fig. VIIIb). In contrast, there was no such effect for control micelles (Fig. VIIIa). As poly(histidine) has been widely utilized as an endosomal escaping material (15), it is not surprising that the imidazole-bearing micelles also showed such capability. Our titration results further verified the buffering ability of imidazole-bearing micelles (Figure S5). When Baf-A1was employed to block the development of endosomes into lysosomes, the phenomenon of endosomal escape of mPEG-PAsp-IM-FITC/Zn^{2+} micelles was not observed, resulting in a reduced cytotoxicity compared to that without Baf-A1co-treatment (Figure S6).

CONCLUSION

In this study, a simple Zn^{2+} crosslinked imidazole-bearing micellar nanocarrier was produced, which could enable charge reversal, endosomal escape, and on-demand cargo release. The imidazole-bearing micelles reversed charge from negative to positive when responding to the acidic tumor microenvironment and enhanced the cellular uptake. After cellular internalization, the endosomal escape was achieved due to the proton sponge effect of imidazole. Although it is challenging to assess the *in situ* SN-38 release kinetics in live cells, the *in vitro* release data revealed rapid drug liberation under acidic conditions. Therefore, drug-loaded imidazole-bearing micelles showed a concurrent drug release and endosomal escape, which could theoretically speed up the onset of therapeutic action of SN 38. The current work provides a solution to the dilemma of nanomedicine complexity and clinical translation, and opens avenues of engineering multifunctional drug delivery nanocarriers without complicated particle architecture in attempt to advance the clinical application of nanomedicines.

Funding Information The work was financially supported by the National Natural Science Foundation of China (21650110447), State Key Laboratory of Medicinal Chemical Biology (Nankai University) (2017030), and the innovation fund of Tianjin University (1706).

REFERENCES

1. Peer D, Karp JM, Hong S, Farokhzad OC, Margalit R, Langer R. Nanocarriers as an emerging platform for cancer therapy. Nat Nanotechnol. 2007;2:751–60.
2. Min Y, Caster JM, Eblan MJ, Wang AZ. Clinical translation of nanomedicine. Chem Rev. 2015;115:11147–90.
3. Estanqueiro M, Amaral MH, Conceicao J, Sousa Lobo JM. Nanotechnological carriers for cancer chemotherapy: the state of the art. Colloids Surf B Biointerfaces. 2015;126:631–48.
4. Blanco E, Shen H, Ferrari M. Principles of nanoparticle design for overcoming biological barriers to drug delivery. Nat Biotechnol. 2015;33:941–51.
5. Cheng Z, A Zaki A, Hui JZ, Muzykantov VR, Tsourkas A. Multifunctional nanoparticles: cost versus benefit of adding targeting and imaging capabilities. Science 2012; 338:903–910.
6. Zhang Z, Yin L, Tu C, Song Z, Zhang Y, Xu Y, et al. Redox-responsive, core cross-linked polyester micelles. ACS Macro Lett. 2013;2:40–4.
7. Torchilin VP. Multifunctional, stimuli-sensitive nanoparticulate systems for drug delivery. Nat Rev Drug Discov. 2014;13:813–27.
8. Lammers T, Aime S, Hennink WE, Storm G, Kiessling F. Theranostic nanomedicine. Acc Chem Res. 2011;44:1029–38.
9. Cha R, Li J, Liu Y, Zhang Y, Xie Q, Zhang M. Fe_3O_4 nanoparticles modified by CD-containing star polymer for MRI and drug delivery. Colloids Surf B Biointerfaces. 2017;158:213–21.
10. Barenholz Y, Peer D. Liposomes and other assemblies as drugs and nano-drugs: from basic and translational research to the clinics. J Control Release. 2012;160:115–6.
11. Louage B, De Wever O, Hennink WE, De Geest BG. Developments and future clinical outlook of taxane nanomedicines. J Control Release. 2017;253:137–52.
12. Bauman JE, Wang JC. Imidazole complexes of nickel(II), copper(II), zinc(II), and silver(I). Inorg Chem. 1964;3:368–73.
13. Yu C, Gao C, Lü S, Chen C, Yang J, Di X, et al. Facile preparation of pH-sensitive micelles self-assembled from amphiphilic chondroitin sulfate-histamine conjugate for triggered intracellular drug release. Colloids Surf B Biointerfaces. 2014;115:331–9.
14. Li X, Gao M, Xin K, Zhang L, Ding D, Kong D, et al. Singlet oxygen-responsive micelles for enhanced photodynamic therapy. J Control Release. 2017;260:12–21.
15. Wu H, Zhu L, Torchilin VP. pH-sensitive poly(histidine)-PEG/DSPE-PEG co-polymer micelles for cytosolic drug delivery. Biomaterials. 2013;34:1213–22.
16. Boussif O, Lezoualc'h F, Zanta MA, Mergny MD, Scherman D, Demeneix B, et al. A versatile vector for gene and oligonucleotide transfer into cells in culture and in vivo: polyethylenimine. Proc Natl Acad Sci U S A. 1995;92:7297–301.
17. Nel AE, Madler L, Velegol D, Xia T, Hoek EMV, Somasundaran P, et al. Understanding bio-physicochemical interactions at the nano-bio interface. Nat Mater. 2009;8:543–57.
18. Xin K, Li M, Lu D, Meng X, Deng J, Kong D, et al. Bioinspired coordination micelles integrating high stability, triggered cargo

release, and magnetic resonance imaging. ACS Appl Mater Interfaces. 2017;9:80–91.
19. Cabral H, Nishiyama N, Kataoka K. Supramolecular nanodevices: from design validation to theranostic nanomedicine. Acc Chem Res. 2011;44:999–1008.
20. Zhao CL, Winnik MA, Riess G, Croucher MD. Fluorescence probe techniques used to study micelle formation in water-soluble block copolymers. Langmuir. 1990;6:514–6.
21. Yang R, Zhang S, Kong D, Gao X, Zhao Y, Wang Z. Biodegradable polymer-curcumin conjugate micelles enhance the loading and delivery of low-potency curcumin. Pharm Res. 2012;29:3512–25.
22. Huang Y, Tang Z, Zhang X, Yu H, Sun H, Pang X, et al. pH-triggered charge-reversal polypeptide nanoparticles for cisplatin delivery: preparation and in vitro evaluation. Biomacromolecules. 2013;14:2023–32.
23. Yue Y, Jin F, Deng R, Cai J, Dai Z, Lin MC, et al. Revisit complexation between DNA and polyethylenimine-effect of length of free polycationic chains on gene transfection. J Control Release. 2011;152:143–51.
24. Shi J, Schellinger JG, Johnson RN, Choi JL, Chou B, Anghel EL, et al. Influence of histidine incorporation on buffer capacity and gene transfection efficiency of HPMA-co-oligolysine brush polymers. Biomacromolecules. 2013;2013(14):1961–70.
25. Tabushi I, Kuroda Y. Bis(histamino) cyclodextin-zn-imidazole complex as an artificial carbonic anhydrase. J Am Chem Soc. 1984;15:4580–4.
26. Deng J, Wang K, Wang M, Yu P, Mao L. Mitochondria targeted nanoscale zeolitic imidazole framework-90 (ZIF-90) for ATP imaging in live cells. J Am Chem Soc. 2017;139:5877–82.
27. Anderson EB, Long TE. Imidazole- and imidazolium-containing polymers for biology and material science applications. Polymer. 2010;51:2447–54.
28. Torchilin VP. Micellar nanocarriers: pharmaceutical perspectives. Pharm Res. 2007;24:1–16.
29. Hanahan D, Weinberg RA. Hallmarks of cancer: the next generation cell. Cell. 2011;144:646–74.
30. Han SS, Li ZY, Zhu JY, Han K, Zeng ZY, Hong W, et al. Dual-pH sensitive charge-reversal polypeptide micelles for tumor-triggered targeting uptake and nuclear drug delivery. Small. 2015;11:2543–54.
31. Wang Z, Chen C, Liu R, Fan A, Kong D, Zhao Y. Two birds with one stone: dendrimer surface engineering enables tunable periphery hydrophobicity and rapid endosomal escape. Chem Commun. 2014;50:14025–8.
32. Mok H, Park JW, Park TG. Enhanced intracellular delivery of quantum dot and adenovirus nanoparticles triggered by acidic pH via surface charge reversal. Bioconjug Chem. 2008;19:797–801.
33. Shen Y, Zhou Z, Sui M, Tang J, Xu P, Van Kirk EA, et al. Charge-reversal polyamidoamine dendrimer for cascade nuclear drug delivery. Nanomedicine. 2010;5:1205–17.
34. Chen C, Tao R, Ding D, Kong D, Fan A, Wang Z, et al. Ratiometric co-delivery of multiple chemodrugs in a single nanocarrier. Eur J Pharm Sci. 2017;107:16–23.
35. Varkouhi AK, Scholte M, Storm G, Haisma HJ. Endosomal escape pathways for delivery of biologicals. J Control Release. 2011;151:220–8.
36. French AP, Mills S, Swarup R, Bennett MJ, Pridmore TP. Colocalization of fluorescent markers in confocal microscope images of plant cells. Nat Protoc. 2008;3:619–28.